Geostationary Lightning Mapper (GLM) Observations of the Brightest Lightning in the Americas

Michael Peterson[1], Erin Lay[1]

[1] ISR-2, Los Alamos National Laboratory, Los Alamos, New Mexico

Corresponding author: Michael Peterson (mpeterson@lanl.gov), B241, P.O. Box 1663 Los Alamos, NM, 87545

Key Points:

- The most radiant optical lighting emissions are referred to as "superbolts."
- Modern orbital measurements are used to identify exceptionally-bright lightning across the Americas.
- The brightest flashes on the continent are largely +CG strokes from mesoscale lightning >100 km in extent.

LA-UR 20-23146

Abstract

Two years of Geostationary Lightning Mapper (GLM) science data are used to document the brightest lighting flashes observed on the Americas continent. The most radiant optical lightning emissions – termed "superbolts" – were first identified by our Vela satellite constellation in the 1970s (Turman, 1977) and are defined in terms of peak optical power. GLM is an integrating sensor that, instead, measures the total optical energy from a lightning pulse. While GLM might not correctly classify short-duration energetic superbolts, its top lightning cases certainly fall in the superbolt category, and the wealth of GLM measurements over its stationary hemispheric field of view provide an unmatched sample of extraordinarily bright lightning.

While radiant bolts in excess of 100x the optical energy of typical lightning are ubiquitous across the Americas and result from many types of lightning processes, we find the most radiant cases (>1000x) are concentrated in the central United States and in the La Plata basin in South America. Coincident Earth Networks Global Lightning Network (ENGLN) observations reveal that these extremely bright emissions usually result from +CG strokes with high peak currents in long horizontal flashes outside of the convective core. Single cases of these megaflashes might produce multiple superbolts over their durations.

Plain Language Summary

Where is the brightest lightning in the Americas? The Geostationary Lightning Mapper (GLM) measures the optical energy of lightning from space. We use two years of continuous staring measurements from across the continent to identify the top cases of lightning "superbolts" – optical emissions from lightning that are at least 100x brighter than normal. GLM confirms past findings that a myriad of lighting processes can produce a superbolt: Intracloud pulses and Cloud-to-Ground strokes with a range of peak currents. However, the absolute brightest cases – at least 1000x more energetic than normal – cluster in certain regions that are known for very large thunderstorms. The superbolts in these Mesoscale Convective Systems (MCSs) often occur with "megaflash" lighting that develop horizontally over hundreds of kilometers, and are associated with intense +CG discharges.

1 Introduction

The flash of light that accompanies a lightning discharge is caused by the dissociation, excitation, and recombination of atmospheric constituents in the hot lightning channel (summarized in Christian et al., 2000). The total radiated optical energy is thought to depend on how much electrical current is flowing down the channel and the channel length (Guo and Krider, 1982; Idone and Orville, 1985; Wang et al., 2005; Qie et al., 2011; Carvalho et al., 2015; Quick et al., 2017). However, while good agreement has been found in ground-based measurements with an unobstructed view of the natural or rocket-triggered Cloud-to-Ground (CG) stroke, space-based measurements of lighting energy are complicated by absorption and scattering in the cloud layer between the source and the satellite. Scattering in the intervening cloud layer dilutes the optical signals in space and delays and broadens them in time (Thomson and Krider, 1982; Koshak et al., 1994; Light et al., 2001a). Radiation scattered away from the instrument or absorbed in the cloud prevent orbital sensors from accurately reconstructing the true power radiated by the source.

Extraordinarily bright optical lightning emissions have been recorded from space since the 1970s (Turman, 1977). These so-called “superbolts” were measured by the optical payload on our Vela constellation of satellites, whose highly-elliptical orbit at 118,000 km altitude provided broad coverage of all lightning-producing regions on Earth. So, what causes these powerful optical signals? Turman (1977) suggested that they could result from CG flashes with intense peak currents or they could be due to measurement bias. Optical lightning signals that do not travel through a thick cloud layer will not be broadened in time, which can increase the peak optical power of an otherwise-normal event to superbolt levels (10^{11} W). One likely scenario for this to occur is when the satellite is at a low elevation angle relative to the source. A satellite near

the horizon might have an unobstructed view below the cloud, allowing it to record the undiluted optical emissions form CG strokes.

In a related study, we are using 12 years of photodiode detector (PDD: Kirkland and Suszcynsky, 2001) observations from the Fast On-orbit Recording of Transient Events (FORTE: Jacobson et al., 1999; Light et al., 2001b) satellite to examine powerful superbolts (source power $>10^{11}$ W). This analysis expands on Kirkland's (1999) analysis of PDD data during the FORTE mission to include the full PDD record that spanned 12 years of observations (1997-2010). However, even with this long PDD record, the FORTE satellite was still limited by its Low Earth Orbit (LEO) snapshot view of thunderstorms around the world. It was thus poorly-suited for recording the extraordinarily rare brightest optical emissions form lightning.

Surveying the brightest lighting flashes requires continuous hemispheric-scale coverage of the Earth. NOAA's new Geostationary Lightning Mappers (GLMs: Goodman et al., 2013; Rudlosky et al., 2019) on the Geostationary Operational Environmental Satellites (GOES) meet this need with one key caveat: as integrating instruments with 2-ms frames, they do not report peak power, but instead measure total optical energy. We can thus use GLM data to identify the most energetic optical lightning signals, but not the most instantaneously powerful signals. FORTE PDD data have shown that total optical energy correlates with peak power (i.e., Kirkland, 1999), but using total energy to screen for the brightest lightning cases will miss short-duration yet extremely powerful optical pulses.

Reporting total energy in a 2-ms integration frame additionally has the potential to make GLM measurements more sensitive to channel length than the peak power in Kirkland's (1999, 2001) 15-microsecond FORTE PDD samples. The Lightning Imaging Sensor (LIS: Christian et al., 2000; Blakeslee et al., 2014) that preceded GLM measured waves of optical energy

104 propagating down established long horizontal lightning channels over 10s of kilometers during
105 multiple consecutive 2-ms LIS frames. These waves occurred at typical speeds of 10^5-10^6 ms^{-1}
106 (Peterson et al., 2018). If we consider this behavior to also occur at higher speeds (perhaps 10^7
107 ms^{-1}), the PDD samples would describe the propagation in 0.15 km increments while LIS / GLM
108 would integrate 20 km of propagation into a single frame. The incremental PDD optical power
109 might remain low while the continuous emission over time results in a single energetic GLM
110 group.

111 Our analysis of the most energetic GLM lightning will complement Turman's (1977)
112 analysis of the most powerful lightning by highlighting cases of strong illumination over long
113 periods of time (hundreds of microseconds to milliseconds). We anticipate that the GLM sample
114 will consist of more stratiform megaflash lighting cases (Lyons et al., 2019) than Turman's
115 analysis (particularly, high peak current +CGs), causing the geospatial distribution of energetic
116 superbolts to shift towards the Americas hotspots for Mesoscale Convective Systems (MCSs).
117 Following our FORTE PDD peak optical power results (Peterson and Kirkland, 2020), we
118 further expect that superbolts resulting from normal lightning that happens to have a relatively
119 clear sight line to the sensor will be frequent at lower energy levels (near the minimum superbolt
120 threshold), while the most energetic superbolts will be almost exclusively +CGs.
121

122 **2 Data and Methodology**

123 2.1 Geostationary Lightning Mapper (GLM) Data

124 GLM superbolts are identified in the GOES-16 data taken from 1/1/2018 - 1/15/2020.
125 We use the post-processed "reclustered" GLM science data (Peterson, 2019) rather than the

operational data produced by the GLM ground system and distributed by NOAA because it includes the following features:

(1) Accurate descriptions of complete and distinct lightning flashes that are not split into multiple features, as in the operational data

(2) Improved solar artifact removal (Peterson, 2020)

(3) Availability of new cluster feature levels including "series" (Peterson and Rudlosky, 2018) describing periods of sustained emission during a flash and "areas" approximating thunderstorm snapshots

(4) Availability of new gridded GLM products including Convective Cloud Probability (Peterson et al., 2020a).

Beyond these and other improvements, the reclustered GLM data is identical to the operational data. Most importantly, it preserves and expands upon the full GLM cluster feature hierarchy. Individual illuminated pixels on the CCD imaging array during a single 2-ms integration frame are termed "events". These events are clustered into "group" features that describe contiguous illuminated regions on the imaging array that approximate the emissions from a lightning pulse. Groups whose constituent events are close in space and time are clustered into lightning "flash" features. Group-to-flash clustering is performed using a Weighted Euclidean Distance (WED) model in geolocated space described in Mach et al., (2020). Our series and area features are then defined from these standard GLM features. Series describing sustained optical emission consist of any collection of groups within the same flash that have no more than one 2-ms empty frame

between them. Our GLM definition of areas, meanwhile, cluster nearby flashes into 15-minute thunderstorm snapshots using a similar WED technique as the group-to-flash clustering.

2.2 Earth Networks Global Lightning Network (ENGLN) Data

The contemporary ENGLN record for the GOES-16 GLM coverage domain and time period of interest is acquired from Earth Networks to provide information on the individual strokes and cloud pulses that correspond to GLM groups, series, and flashes. ENGLN is a distributed heterogeneous network of long-range ground-based Radio-Frequency (RF) lightning sensors that consists of Earth Networks Total Lightning Network (ENTLN: Zhu et al., 2017) and World-Wide Lightning Location Network (WWLLN: Jacobson and Holzworth, 2006; Hutchins et al., 2012) stations. ENGLN geolocates lightning sources and additionally reports their type (CG or IC) and peak current (including polarity). There is a caveat with the reported polarity of CG strokes, however. In +CG cases far from the reporting sensors where the ground wave is attenuated, the network may geolocate based on the sky wave. For this reason, in these situations the polarity accuracy is improved by reporting those +CG events as -CGs (Stock 2020, personal communication). Thus, some of the –CG events coincident with GLM superbolts that we report might, in fact, be misclassified +CGs.

The ENGLN stroke data is ingested into the GLM flash clustering hierarchy at the event level. We only use the subset of the GOES-16 GLM record with the current timing accuracy (starting after the 10/15/2018 software update) to collocate with ENGLN. We define ENGLN strokes to be “events” that are the children of GLM groups, grandchildren of GLM series, and great-grandchildren of GLM flashes. For an ENGLN stroke to be assigned to a GLM flash, it must occur within a 10-km ring around the flash footprint, and within the time window that starts

330 ms before the first GLM event and ends 330 ms after the last GLM event. We base our collocation method on events rather than group or flash centroid locations (as in Rudlosky et al., 2017) because we assume that all ENGLN sources within ~1 GLM pixel of the illuminated cloud region are contributing to the optical energies recorded by GLM.

For an ENGLN event to be assigned to a GLM series, it must first be assigned to the parent flash and then occur within a 2-ms window encompassing the series start and end times. Finally, we assign the ENGLN event to the most radiant GLM group that occurs within 3 integration frames of the reported event time. This allows us to associate the ENGLN source with the peak of the GLM light curve from superbolt cases rather than the instantaneous optical energy at the time of source occurrence. It is not intended as a matching scheme that should be applied for other applications (for example, determining relative Detection Efficiency).

2.3 Identifying GLM Superbolts

Turman's (1977) original superbolts were identified in half-millisecond scale optical waveform records from a non-imaging photodiode detector. The most appropriate point of comparison with GLM is the group feature that integrates all recorded energy over the illuminated cloud region during a single 2-ms frame. Turman (1977) described superbolts as being "over 100x more intense than typical lighting" in addition to providing optical peak power thresholds and quantifying their frequencies. We base our GLM superbolt definition on this ">100x more intense" description rather than calculating the energy radiated by the source because it allows us to side-step differences in viewing geometry, instrument sensitivity, and pixel size across the GLM CCD array. For a GLM group that occurs at a specific location to be considered a superbolt, it must exceed the mean energy for all groups at that location (that

illuminate the same portion of the GLM CCD array and have the same source-to-satellite look angles) by a factor of at least 100.

Figure 1 shows the magnitude of these differences in GLM energy across its Field of View (FOV). The average energy of the dimmest event per flash is plotted in Figure 1a on a 0.1 degree grid. The dimmest event energy approximates the minimum threshold for detection. At the center of the imaging array, events as low as 1-2 fJ are routinely detected by GLM. However, this threshold increases radially from the satellite subpoint. The average minimum detected energy per flash exceeds 30 fJ by the edge of the instrument FOV.

Superimposed on this behavior are quasi-horizontal lines of reduced minimum event energies compared to surrounding rows of pixels. These linear features correspond to the boundaries of the Real Time Event Processors (RTEPs) that comprise the imaging array. These boundaries and the performance of certain RTEPs can be problematic for identifying superbolts in absolute units. Figure 1b demonstrates this by showing the average energy of the most radiant group per flash on the same grid. As in Figure 1a, intensity of the brightest groups per flash increases at the limb, which is attributed to the side view of the thunderstorms in these regions. Unlike Figure 1a, details of the lightning distribution can be noted in Figure 1b. These include land / ocean differences in optical energy and peaks in group energy along the Andes mountains. However, the most notable variations in Figure 1b encompass two RTEPs that feature severely increased maximum group energies over part or all of their spatial domains (manifest as red rectangles): one located at 90º W, 20º S, and the other at 90º W, 50º S. If we determined a

superbolt threshold based on the mean energy normalized to the source, then a large fraction of the groups in these boxes would be incorrectly identified as superbolts.

Instead, we base our minimum superbolt threshold on the average flash mean group energy plotted in Figure 1c. This grid still has some of the terrain-based differences in lightning radiance from Figure 1b, but it highlights variations in group energy based on RTEP performance and look angle. To reduce spatial biases across the center of the GLM CCD array, we impose a minimum local superbolt threshold equal to 100x the average energy of all GLM groups of 1167 fJ. Any pixel whose average group energy falls below this value will be assigned a threshold of 1167 fJ. Superbolt group energy thresholds are plotted in Figure 1d. The local thresholds vary by less than a factor of 2 across most land-based regions in the center of the GLM FOV, are higher over oceanic regions, and increase rapidly at the limb. Groups in the problematic RTEP regions discussed previously are suppressed by high threshold values in Figure 1d that reach 25,000 fJ.

We apply these thresholds to all GLM groups between 1/1/2018 and 1/15/1020 in the reclustered GLM dataset. To remove residual solar contamination, we further enforce a maximum superbolt rate of 50 superbolts per 15-minute data file. Files with rates exceeding this limit are deemed to be contaminated and skipped. This leaves us with 2,021,554 GLM superbolts that exceed the typical energy of local lightning activity by at least a factor of 100 out of the 11

228 billion groups observed by GLM during this period. For comparison, the FORTE PDD detected
229 20,000 100-GW superbolts over its 12 years in operation.

230

231 **3 Results**

232 In the following sections, we examine common types of lightning that produce superbolts
233 (Section 3.1), and then analyze the frequency of GLM superbolts and where they are located
234 (Section 3.2). Finally, we focus on superbolts that match ENGLN events to determine how
235 superbolts are divided between IC and CG cases, and how they relate to the behavior of the
236 parent flash.

237

238 *3.1 Types of GLM Optical Superbolts*

239 While it is possible for many types of lightning processes to generate superbolts
240 (especially at lower energy levels), there are two common scenarios in which they occur
241 (Peterson et al., 2020b). "Anvil superbolts" are cases where the lightning illuminates primarily
242 the clouds at the edge of the storm – often forward anvils in MCS thunderstorms. A GLM
243 example of an anvil superbolt that had ENGLN coincidence is shown in Figure 2. The central
244 panel plots the GOES-16 Advanced Baseline Imager (ABI: Schmit et al., 2017) longwave
245 infrared (CH14) product on top of NASA Earth imagery (Stockli et al., 2005) and then allows
246 GLM events to "illuminate" the cloud (i.e., brighten the image). On top of the event data, the
247 progression of groups over time is drawn as line segments connecting each group centroid to its
248 nearest preceding neighbor. The longitude extent (top) and latitude extent (right) of each group
249 in sequential order are also shown on the outer panels and timeseries of normalized group energy

(top) and area (bottom) are plotted along the bottom of the figure. ENGLN CG strokes (asterisk symbols) and IC pulses (diamond symbols) are also plotted with peak currents listed (in kA). The symbol color indicates polarity with negative colored blue and positive red.

This anvil flash featured a superbolt that was 1000x more energetic than typical lightning in the La Plata basin in Argentina. The superbolt resulted from a –CG stroke with a peak current of -163 kA. The strong peak current combined with the flash location at the edge of the storm allowed its optical energy to reach such a high level. The storm region where the superbolt was centered had more groups supplied by propagating flashes (> 50 km in lateral extent) than non-propagating flashes, resulting in the superbolt centroid being assigned a non-convective cloud type (Peterson et al., 2020a). Anvil superbolts may be labeled as convective or non-convective, depending on where the radiance-weighted centroid is located. The defining characteristic of this type of lighting is that it illuminates clouds near the edge of the storm – where we expect to find favorable sight lines to the sensor that might allow normal lightning to be identified as a superbolt.

The other common scenario for superbolts to occur is the case of highly-radiant groups in long-horizontal stratiform flashes. An example of a megaflash with a 1000x superbolt group is depicted in Figure 3 following the same convention a Figure 2. The ENGLN events trace out all of the major branches of the GLM flash as it propagates northward. The first two seconds of this flash produced only IC activity in the ENGLN data. The flash went on to put down 27 CG strokes over the course of ~5 s at various points along its branched structure. 14 of these stokes were +CGs with peak currents ranging from +26 kA to +233 kA. The remaining 13 –CGs all had peak currents < 16 kA. The 1000x superbolt group occurred during the +233 kA CG located in the northwestern branch of the flash. What makes these stratiform superbolt cases different form

anvil superbolts is that the layered homogeneous nature of stratiform clouds prohibits a "shortcut" explanation for why these superbolts are recorded to be so energetic. The lightning, itself, has to be exceptional in some way – which is why we expect to see +CGs with high peak currents (as in this case) frequently corresponding to energetic GLM superbolts. Not only are these +CGs intense, but +CGs are also known to produce broader waveforms (Light et al., 2001b) that should result in greater total optical energies than the comparably quick –CGs.

3.2 Frequencies and Locations of GLM Superbolts

Table 1 categorizes our 2 million GLM superbolt groups according to energy threshold level and prevailing GLM cloud type. Percentiles are shown according to the number of GLM groups and flashes in the sample. While the group percentiles are representative of the brightness of superbolt groups compared to all types of lightning emissions, in general, we focus on the flash percentiles because the former optical instruments preferentially detected the brightest optical emissions per flash. The FORTE PDD, for example, might only see a single trigger from the return stroke in a flash. Most GLM groups, by contrast, describe dim cloud pulses that map out the lateral development of the flash over time. As such, GLM flashes exist that individually consist of tens of thousands of groups, and these faint cloud pulses inflate the apparent significance of superbolt groups. The flash percentiles are a better point of comparison for superbolt frequency because none of the previous optical instruments match the trigger rates of GLM.

At the 100x energy level, we are capturing GLM groups in the 99.68^{th} percentile of flashes with three out of every four groups occurring in convective clouds. This sample is

relatively generous compared to Turman's (1977) 10^{11} W superbolts, which accounted for the 99.8th percentile of lightning. Increasing the GLM energy threshold to 117x matches this proportion (though not, necessarily, the sample composition as noted previously).

Table 1 further lists energy thresholds that correspond to incremental factors of 250x and also factors that bring the flash percentile an order of magnitude closer to 100% (99, 99.9, 99.99 etc.). While the sample size diminishes as the threshold increases, the number of non-convective superbolts does not fall off as fast as the number of convective cases. Convective and non-convective superbolts reach parity at thresholds around 250x, while non-convective cases dominate the highest thresholds. The GLM threshold that matches the proportion of the lightning sample from Turman's (1977) higher $3x10^{12}$ W superbolt threshold (817x) contains 274 non-convective cases and only 46 convective cases, and non-convective superbolts outnumber convective superbolts ten-to-one at 1000x.

Figure 4 shows how 100x (top row) and 500x (bottom row) superbolts are distributed across the continent (left column) and the mean convective cloud probability for the region of their parent thunderstorms that they illuminate (right column). The locations of 1000x superbolts are also drawn as red box symbols in Figure 4c. Superbolt frequency in Figure 4a and c is plotted as a Group Extent Density (GED) where each gridpoint that is illuminated by a single group is incremented by one. These counts include all GLM data from 1/1/2018 until 1/15/2020. Boxes are also shown that outline regions of interest that will be considered in subsequent analyses.

At the 100x energy threshold level, superbolts are ubiquitous across the GLM FOV. The superbolt frequency mirrors the GLM lightning distribution (Peterson, 2019) with more superbolts over land than ocean and terrain-induced hotspots in mountainous and coastal regions

317 across the continent. In most regions, 100x superbolts primarily come from convective clouds
318 (Figure 4b). There are three key exceptions, however: the central United States, the La Plata
319 basin in South America, and various oceanic regions where artifacts or anomalies are common.
320 All three report superbolts in primarily non-convective cloud types (< 50% in Figure 4b). The
321 first two regions are known for frequent MCS activity where we expect to find stratiform
322 superbolts. The third case includes the two problematic RTEPs discussed previously as well as
323 regions near the edge of the GLM FOV where solar contamination is common. While Figure 4a
324 shows that we have removed most of these issues, the remaining cases still stand out in Figure 4b
325 because they generate small numbers of long-duration flashes that cover large regions on the
326 GLM CCD array. This makes them look like lightning in non-convective clouds. For this reason,
327 we will ignore these oceanic regions in the following analyses.

328 As we increase the energy threshold beyond 100x, the contiguous superbolt distribution
329 over the continent from Figure 4a erodes, leaving key hotspot regions for energetic superbolt
330 activity. Figure 4c shows that the highest concentrations of 500x superbolts (color contour) and
331 almost all cases of 1000x superbolts (red box symbols) are located in the central United States, in
332 the La Plata basin in South America, and in Central America between the Colombian coast and
333 southern Mexico. There are also two 1000x superbolts in the Andes region, two cases in the
334 Midwest, and one case in New York. The remaining red boxes in Figure 4c are suspected to be
335 artifacts and ignored. Non-convective cloud types prevail for these particularly energetic
336 superbolts with large swaths of red (25% convective probability) apparent in Figure 4d –
337 especially over the Great Plains and eastern La Plata basin.

338 The increase in non-convective lightning frequency with increasing superbolt energy
339 threshold is not unique to the two MCS hotspot regions, however. Figure 5 plots the fraction of

non-convective superbolts as a function of superbolt threshold in all six boxed regions from Figure 4. While the La Plata basin and the Great Plains (both depicted with dashed lines) are predisposed towards non-convective superbolts at all energy levels compared the other regions, all regions depicted in Figure 5 feature increasing proportions of non-convective lightning with increasing superbolt threshold. Regardless of region, the top energetic cases (>1000x) almost exclusively occur in non-convective clouds.

Figures 4 and 5 demonstrate that the most energetic GLM superbolts occur in thunderclouds with propagating flash activity, but they do not associate these exceptionally-energetic groups with long horizontal megaflashes. To determine whether megaflashes are responsible for these superbolts, we identify the parent flashes for these groups in the GLM clustering hierarchy and then construct histograms for flash extent – defined as the maximum great circle distance between groups. Separate histograms are constructed for each threshold level between 100x and 1500x. Figure 6 shows these histograms as a two-dimensional contour plot. Each bin in the figure represents one histogram with frequencies totaling 100%. Median values are shown with a solid line while the 25th and 75th percentiles are shown with dashed lines. In order to increase the number of samples at higher threshold levels, we include superbolts in all regions that are not near the edge of the GLM FOV or over the southern Pacific Ocean where the problematic RTEPs are located.

The median and quartile curves in Figure 6 increase considerably over the range of superbolt energy thresholds shown. At 100x, the median flash extent is 33 km, but it increases to 200 km by 1000x. Megaflashes are loosely defined as lightning whose extent exceeds 100 km. The quartile curves show that 75% of the sample of 100x superbolts are not megaflashes because their extents are shorter than 100 km. However, the reverse is true for 1000x superbolts, and

363 75% of their parent flashes exceed the 100 km megaflash threshold. Due to the slope of the
364 curve, this statement is also true for less-energetic superbolts – even as low as ~600x. The
365 changeover point from mostly non-megaflashes to mostly megaflashes is at the ~300x energy
366 level.

367

368 *3.3 GLM and ENGLN Statistics of Matched Superbolt Groups*

369 We integrate ENGLN measurements into the GLM flash clustering hierarchy to provide
370 further insights into what the parent lightning flash is doing and which lightning processes are
371 responsible for the energetic GLM optical superbolts. We limit our analysis to the most recent
372 period of the GLM record with accurate timing information (10/16/2018 – 1/15/2020). GLM
373 superbolt and ENGLN matches are summarized in Table 2. This 14-month period contained
374 575,455 GLM superbolts that exceeded the 100x energy threshold level, and 115,304 of these
375 were successfully matched to an ENGLN event. 85% of these matches were to CG strokes, with
376 the remaining 15% coming from IC pulses. Most of these matched GLM superbolts occurred in
377 convective clouds (64% for CGs, 56% for ICs).

378 Figure 7 uses the matched cases to construct histograms (bar plots) and Cumulative
379 Distribution Functions (CDFs; solid lines) for the duration of the series containing CG (blue) and
380 IC (red) superbolts (top row), and the superbolt multiplicity per flash (bottom row). These
381 distributions are partitioned between convective cases (left column) and non-convective cases

382 (right column). GLM series document periods of sustained optical emission from a lightning
383 flash. Thus, the series that contained the superbolt describe the light curve from the event.

384 Convective superbolt series (Figure 7a) typically last tens of milliseconds. Following the
385 analysis in Bitzer (2017), these series might describe continuing current associated with the
386 superbolt event; however, there is little difference between CG and IC cases (as noted in the
387 CDFs). The non-convective superbolt cases (Figure 7b) occur in series that are considerably
388 longer – lasting up to hundreds of milliseconds. CG cases also have slightly shorter durations
389 than their IC counterparts.

390 Almost all superbolt flashes contain only a single CG or IC superbolt group (Figure 7c-
391 d). However, there are still thousands of cases of flashes in our matched sample that produce
392 multiple superbolts. Convective cases (Figure 7c) contain at most 5 superbolt groups. It is
393 possible that continuing current in a superbolt CG could generate sustained emission above the
394 100x level for multiple GLM groups. However, that is not what is occurring here because we are
395 looking at superbolt groups with ENGLN matches and ENGLN strokes are only assigned to one
396 group in a given flash (i.e., the brightest group at the peak of the light curve). The cases of
397 superbolt multiplicity in a given flash from Figure 7c-d are subsequent strokes. Superbolt
398 multiplicity is more common in non-convective cases than in convective cases, where a single
399 flash can contain as many as 10 distinct CG or IC ENGLN events that produce GLM superbolts.

400 Figure 8 compares the number of CG and IC superbolts. Histograms are shown in Figure
401 8a-b while the IC fraction of each bin is computed in Figure 8c-d. As before, convective cases
402 are shown in the left column while non-convective cases are shown in the right column. While
403 the fraction of non-convective cases increases with superbolt threshold, as we saw previously,

404 the IC fraction remains between 10-20% for all bins < 1000x. All matched cases exceeding
405 1000x are CGs.

406 The polarity and peak current distributions do change according to GLM superbolt
407 energy threshold, however. Figure 9 shows histograms and CDFs for 100x CG superbolts
408 (Figure 9a-b) and 500x CG superbolts (Figure 9 e-f) in convective (left) and non-convective
409 (right) clouds. Here, we see the key difference between the superbolts in each cloud type.
410 Superbolts in convective clouds are dominated by –CGs, while the majority of superbolts in non-
411 convective clouds are +CGs. In both cases, the +CGs that produce superbolts at the 100x level
412 tend to be stronger than their –CG counterparts. The median of the +CG CDF is 10 kA greater
413 than the –CG median for convective clouds (Figure 9a), and 15 kA greater for non-convective
414 (Figure 9b).

415 Increasing the GLM superbolt threshold to 500x eliminates the ENGLN matches with
416 weak (< 20 kA) peak currents, shifting all of the histograms in Figure 9c-d towards cases of
417 100+ kA CGs. There are 20 cases of GLM superbolts at the 1000x level with ENGLN matches:
418 two convective superbolts (1 +CG and 1 –CG, both > 80 kA) and 18 non-convective superbolts
419 (16 +CGs and 2 –CGs, all > 50 kA). These +CG non-convective superbolts include some of the
420 top peak current cases in the distributions from Figure 9b and d. This analysis demonstrates that
421 the lower end of the superbolt distribution (>100x) includes many cases of what we would
422 expect from "normal" CG lightning (-CGs with peak current < 20 kA located in convective
423 clouds). Thus, normal lightning can be a superbolt in certain scenarios. However, as we move up
424 in GLM energy, these "normal" cases fade away, leaving a sample that contains increasing
425 fractions of exceptional +CG cases from non-convective cloud regions.
426

4 Conclusion

This study documents the top cases of energetic GLM lightning on the Americas continent. While these superbolt cases account for the top 0.33% of GLM groups at the 100x energy threshold, the integrating nature of the GLM instrument over its 2-ms frames will result in discrepancies with the former Turman (1977) analysis, which defined superbolts based on the peak power of optical waveforms that had microsecond-scale precision. In particular, long-duration pulses are expected to be more prevalent in the GLM record than particularly intense optical pulses with short durations.

At the 100x energy threshold level, GLM superbolt groups are ubiquitous across the continent, come from primarily convective thunderstorm regions, and cases with matching ENGLN CG events are dominated by –CGs with a typical range of peak currents (median: 8 kA). However, as the energy threshold increases, the proportion of these "normal" lightning events diminishes. By 500x, the superbolt distribution clusters into hotspot regions over the central United States, the La Plata basin in South America, and coastal regions of Central America. The sample becomes dominated by megaflashes in non-convective regions of the parent thunderstorm, and cases with ENGLN matches have higher peak currents (medians: 90-100 kA) with the sample consisting mostly of +CGs.

This transition from weaker GLM cases resulting from many types of lightning to stronger GLM cases originating from +CGs with high peak currents agrees with our previous FORTE analysis that identified superbolts according to peak optical power, yet FORTE did not identify hotspots over land-based regions with abundant MCS and megaflash activity. It is unclear whether this is due to the difference between peak optical power and total energy, or if the rarity of megaflash events caused them to be overlooked in the historical optical superbolt

analyses. To date, not a single megaflash case with an extent >100 km has been recorded by a lighting imager in Low Earth Orbit (LEO). Only instruments in geosynchronous orbit are able to identify large megaflashes on a routine basis. The global GLM superbolt hotspots also differ from the global distribution of the most energetic RF lightning strokes discussed by Holzworth et al. (2019). While these WWLLN event are termed "superbolts," they are not, necessarily, the same events identified by optical means. The peak of the RF energy distribution represents a third category to the Vela / FORTE peak optical power superbolts and the GLM total energy superbolts.

Future work will compare GLM measurements of these superbolt flashes with RF and high-speed optical measurements from our upcoming SENSER payload that is slated for a geosynchronous mission in a western hemisphere slot. These combined measurements will allow us to reconcile Turman's (1977) superbolts with modern optical measurements. We also plan to use our RF and optical instrumentation to reconcile the WWLLN RF superbolts with the peak optical power and total optical energy superbolts.

Acknowledgments

This work was supported by the US Department of Energy through the Los Alamos National Laboratory. Los Alamos National Laboratory is operated by Triad National Security, LLC, for the National Nuclear Security Administration of U.S. Department of Energy (Contract No. 89233218CNA000001). The GLM LCFA and ABI data sets may be obtained from NOAA via their CLASS service, which is located at https://www.class.noaa.gov/ (GLM:

https://www.avl.class.noaa.gov/saa/products/search?datatype_family=GRGLMPROD, ABI: https://www.avl.class.noaa.gov/saa/products/search?datatype_family=GRABIPRD). The ENGLN data used in this study were provided by Earth Networks, Inc. (https://www.earthnetworks.com/), and may be ordered from them.

References

Bitzer, P. M. (2017), Global distribution and properties of continuing current in lightning, *J. Geophys. Res. Atmos.*, 122, 1033– 1041, doi:10.1002/2016JD025532.

Blakeslee, R. J., H. J. Christian, M.F. Stewart, D.M. Mach, M. Bateman, T.D. Walker, D. Buechler, W.J. Koshak, S. O'Brien, T. Wilson, E.C. Colley, T. Abbott, J. Carter S. Pavelitz, C. Coker, 2014: Lightning Imaging Sensor (LIS) for the International Space Station (ICC): Mission description and science goals, *XV Int. Conf. Atmos. Electricity.* Norman, OK, 15pp.

Carvalho, F. L., Uman, M. A., Jordan, D. M., and Ngin, T. (2015), Lightning current and luminosity at and above channel bottom for return strokes and M-components, *J. Geophys. Res. Atmos.*, 120, 10,645– 10,663, doi:10.1002/2015JD023814.

Goodman, S. J., Blakeslee, R. J., Koshak, W. J., Mach, D., Bailey, J., Buechler, D., ... & Stano, G. (2013). The GOES-R geostationary lightning mapper (GLM). *Atmospheric research*, *125*, 34-49.

Guo, C., and Krider, E. P. (1982), The optical and radiation field signatures produced by lightning return strokes, *J. Geophys. Res.*, 87(C11), 8913– 8922, doi:10.1029/JC087iC11p08913.

Hutchins, M. L., Holzworth, R. H., Brundell, J. B., and Rodger, C. J. (2012), Relative detection efficiency of the World Wide Lightning Location Network, *Radio Sci.*, 47, RS6005, doi:10.1029/2012RS005049.

Idone, V. P., and Orville, R. E. (1985), Correlated peak relative light intensity and peak current in triggered lightning subsequent return strokes, *J. Geophys. Res.*, 90(D4), 6159– 6164, doi:10.1029/JD090iD04p06159.

Jacobson, A. R., Knox, S. O., Franz, R., & Enemark, D. C. (1999). FORTE observations of lightning radio-frequency signatures: Capabilities and basic results. *Radio Science*, *34*(2), 337-354.

Jacobson, A.R., R. Holzworth, J. Harlin, R. Dowden, and E. Lay, 2006: Performance Assessment of the World Wide Lightning Location Network (WWLLN), Using the Los Alamos Sferic Array (LASA) as Ground Truth. *J. Atmos. Oceanic Technol.,* **23**, 1082–1092, https://doi.org/10.1175/JTECH1902.1

Kirkland, M. W. (1999). An examination of superbolt-class lightning events observed by the FORTE satellite. *Los Alamos National Laboratory, Atmospheric Sciences Group, New Mexico*.

Kirkland, M. W., Suszcynsky, D. M., Guillen, J. L. L., and Green, J. L. (2001), Optical observations of terrestrial lightning by the FORTE satellite photodiode detector, *J. Geophys. Res.*, 106(D24), 33499– 33509, doi:10.1029/2000JD000190.

Koshak, W. J., Solakiewicz, R. J., Phanord, D. D., and Blakeslee, R. J. (1994), Diffusion model for lightning radiative transfer, *J. Geophys. Res.*, 99(D7), 14361– 14371, doi:10.1029/94JD00022.

Light, T. E., Suszcynsky, D. M., Kirkland, M. W., and Jacobson, A. R. (2001a), Simulations of lightning optical waveforms as seen through clouds by satellites, *J. Geophys. Res.*, 106(D15), 17103– 17114, doi:10.1029/2001JD900051.

Light, T. E., Suszcynsky, D. M., and Jacobson, A. R. (2001b), Coincident radio frequency and optical emissions from lightning, observed with the FORTE satellite, *J. Geophys. Res.*, 106(D22), 28223– 28231, doi:10.1029/2001JD000727.

Lyons, W. A., Bruning, E. C., Warner, T. A., MacGorman, D. R., Edgington, S., Tillier, C., & Mlynarczyk, J. (2019). Megaflashes: Just How Long Can a Lightning Discharge Get?. *Bulletin of the American Meteorological Society*, (2019).

Mach, D. M. (2020). Geostationary Lightning Mapper clustering algorithm stability. *Journal of Geophysical Research: Atmospheres*, 125, e2019JD031900. https://doi.org/10.1029/2019JD031900

Peterson, M., Rudlosky, S., & Deierling, W. (2018). Mapping the lateral development of lightning flashes from orbit. *Journal of Geophysical Research: Atmospheres*, 123, 9674–9687. https://doi.org/10.1029/2018JD028583

Peterson, M., & Rudlosky, S. (2019). The time evolution of optical lightning flashes. *Journal of Geophysical Research: Atmospheres*, 124, 333– 349. https://doi.org/10.1029/2018JD028741

Peterson, M. (2019). Research applications for the Geostationary Lightning Mapper operational lightning flash data product. *Journal of Geophysical Research: Atmospheres*, 124, 10205– 10231. https://doi.org/10.1029/2019JD031054

Peterson, M. (2020). Removing solar artifacts from Geostationary Lightning Mapper data to document lightning extremes. *Journal of Applied Remote Sensing*, *14*(3), 032402.

Peterson, M., and M. W. Kirkland 2020: Revisiting the detection of lightning superbolts. *J. Geophys. Res.,* this issue (companion paper).

Peterson, M., Rudlosky, S., & Zhang, D. (2020a). Thunderstorm Cloud-Type Classification from Space-Based Lightning Imagers. Monthly Weather Review, (2020).

Peterson, M., Rudlosky, S., & Zhang, D. (2020b). Changes to the appearance of optical lightning flashes observed from space according to thunderstorm organization and structure. *Journal of Geophysical Research: Atmospheres*, 125, e2019JD031087. https://doi.org/10.1029/2019JD031087

Qie, X., Jiang, R., Wang, C., Yang, J., Wang, J., and Liu, D. (2011), Simultaneously measured current, luminosity, and electric field pulses in a rocket-triggered lightning flash, *J. Geophys. Res.*, 116, D10102, doi:10.1029/2010JD015331.

Quick, M. G., and Krider, E. P. (2017), Optical power and energy radiated by return strokes in rocket-triggered lightning, *J. Geophys. Res. Atmos.*, 122, 8816– 8832, doi:10.1002/2017JD027363.

Rudlosky, S.D., M.J. Peterson, and D.T. Kahn, 2017: GLD360 Performance Relative to TRMM LIS. *J. Atmos. Oceanic Technol.,* **34**, 1307–1322, https://doi.org/10.1175/JTECH-D-16-0243.1

Rudlosky, S. D., Goodman, S. J., Virts, K. S., & Bruning, E. C. (2019). Initial Geostationary Lightning Mapper Observations. *Geophysical Research Letters, 46*(2), 1097-1104. doi:10.1029/2018gl081052

Schmit, T. J., Griffith, P., Gunshor, M. M., Daniels, J. M., Goodman, S. J., & Lebair, W. J. (2017). A closer look at the ABI on the GOES-R series. *Bulletin of the American Meteorological Society*, *98*(4), 681-698.

Stöckli, R., Vermote, E., Saleous, N., Simmon, R., & Herring, D. (2005). The Blue Marble Next Generation-A true color earth dataset including seasonal dynamics from MODIS. *Published by the NASA Earth Observatory*.

Thomson, L.W. and E.P. Krider, 1982: The Effects of Clouds on the Light Produced by Lightning. *J. Atmos. Sci.,* **39**, 2051–2065, https://doi.org/10.1175/1520-0469(1982)039<2051:TEOCOT>2.0.CO;2

Turman, B. N. (1977), Detection of lightning superbolts, *J. Geophys. Res.*, 82(18), 2566– 2568, doi:10.1029/JC082i018p02566.

Uman, M. A. (1978), Criticism of "Comment on 'Detection of lightning superbolts' by B. N. Turman" by R. D. Hill, *J. Geophys. Res.*, 83(C11), 5523– 5523, doi:10.1029/JC083iC11p05523.

Wang, D., N. Takagi, T. Watanabe, V. A. Rakov, M. A. Uman, K. J. Rambo, and M. V. Stapleton (2005), A comparison of channel-base currents and optical signals for rocket-triggered lightning strokes, *Atmos. Res*., **76**, 412–422.

Zhu, Y., Rakov, V. A., Tran, M. D., Stock, M. G., Heckman, S., Liu, C., … Hare, B. M. (2017). Evaluation of ENTLN performance characteristics based on the ground truth natural and rocket-triggered lightning data acquired in Florida. *Journal of Geophysical Research: Atmospheres*, 122. 9858– 9866, https://doi.org/10.1002/2017JD027270

583 **Table 1.** GLM superbolt frequency by energy threshold level and prevailing cloud type. The
584 large dataset generated by GLM's staring measurements permits the identification of
585 exceptionally rare highly-energetic superbolt events. Percentiles are shown according to the total
586 number of groups and flashes considered.
587

	Group Percentile	Flash Percentile	Count		
			All	Convective	Non-Convective
100x	99.982	99.68	2,021,554	1,525,251	496,303
Turman 10^{11} W	-----	99.80	-----	-----	-----
117x	99.989	99.80	1,256,664	918,600	338,064
144x	99.994	99.90	626,405	431,951	194,454
250x	99.9993	99.98	72,957	38,518	34,439
258x	99.9994	99.990	63,802	33,058	30,744
438x	99.99994	99.9990	6,349	2,182	4,167
500x	99.99997	99.9994	3,506	1,062	2,444
703x	99.999994	99.99990	641	125	516
Turman $3x10^{12}$ W	-----	99.99995	-----	-----	-----
817x	99.999997	99.99995	320	46	274
1000x	99.999999	99.99998	110	10	100
1100x	99.9999994	99.999990	61	3	58
1500x	99.99999993	99.999999	7	0	7

588
589

590 **Table 2.** ENGLN matches for GLM superbolt groups with accurate timing (10/16/2018 –
591 1/15/2020).
592

	Count		
	All	Convective	Non-Convective
All GLM Superbolts	575,455	362,693	212,762
All ENGLN Matches	115,304	73,671	41,633
ENGLN CG Matches	98,678	64,285	34,393
ENGLN IC Matches	16,626	9,386	7,240

593
594

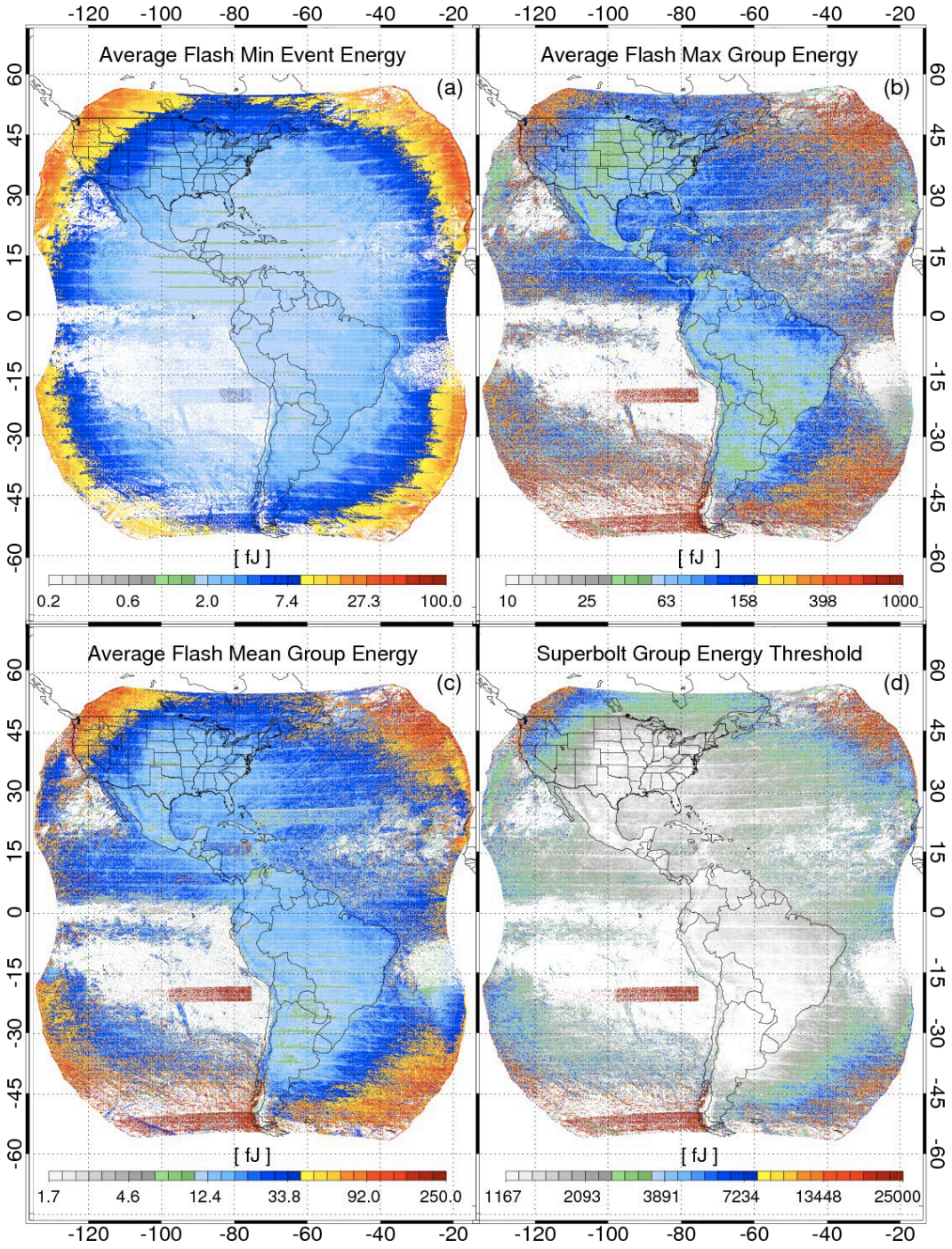

Figure 1. Distributions of GOES-16 GLM energy across its FOV. (a) The average energy of the dimmest event per flash. (b) The average energy of the brightest group per flash. (c) The average group energy. (d) Superbolt energy threshold (at least 100x more radiant than the average local group energy). The floor of the superbolt threshold distribution is capped at 1167 fJ – 100x the overall mean group energy.

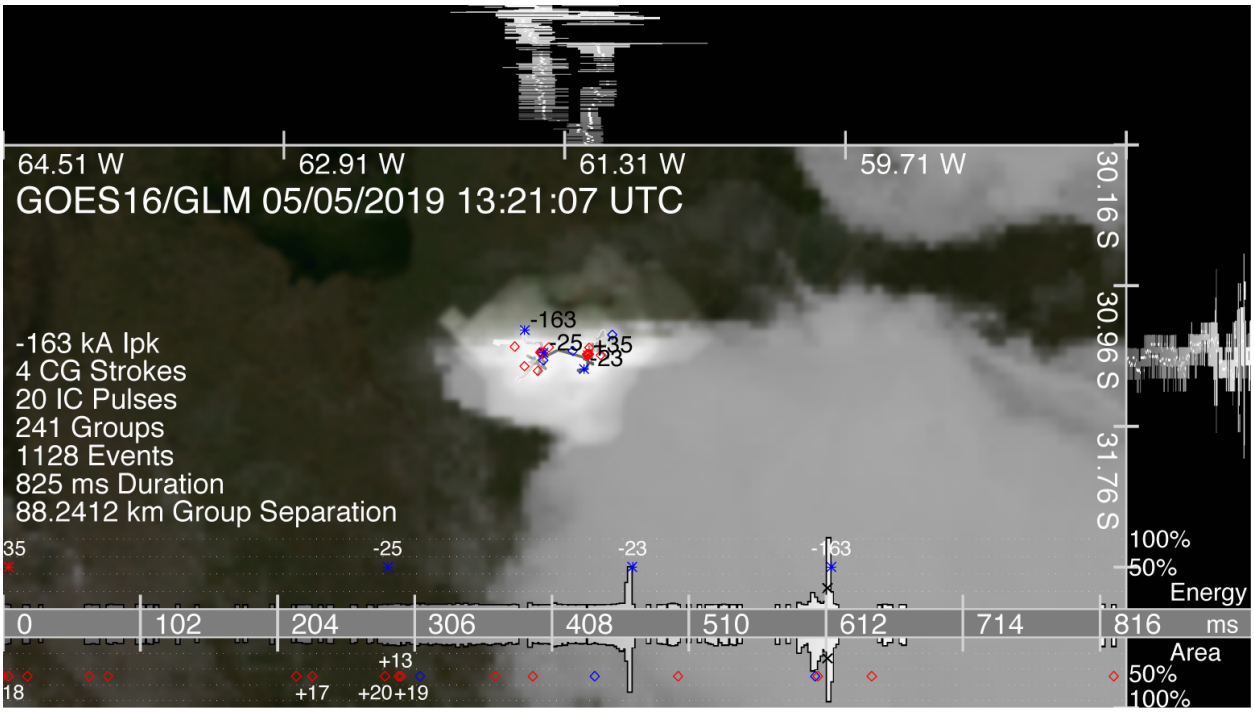

Figure 2. An example 1000x anvil superbolt that occurred at the edge of the parent thunderstorm. ABI CH14 (11.2 μm) infrared imagery is brightened by GLM events according to their energy in the central panel. Greyscale line segments indicate the lateral progression of groups over time. The outer panels show the longitude (top) and latitude (right) extent of each group in sequential order. The bottom timeseries shows normalized group energy (top) and group area (bottom) over the course of the flash. ENGLN CGs (asterisk symbols) and ICs (diamond symbols) are shown in the central panel and the timeseries with negative (positive) polarity events colored blue (red). Peak currents are displayed for IC events > 10 kA and all CG events. The 1000x superbolt group is indicated in the timeseries with an X symbol.

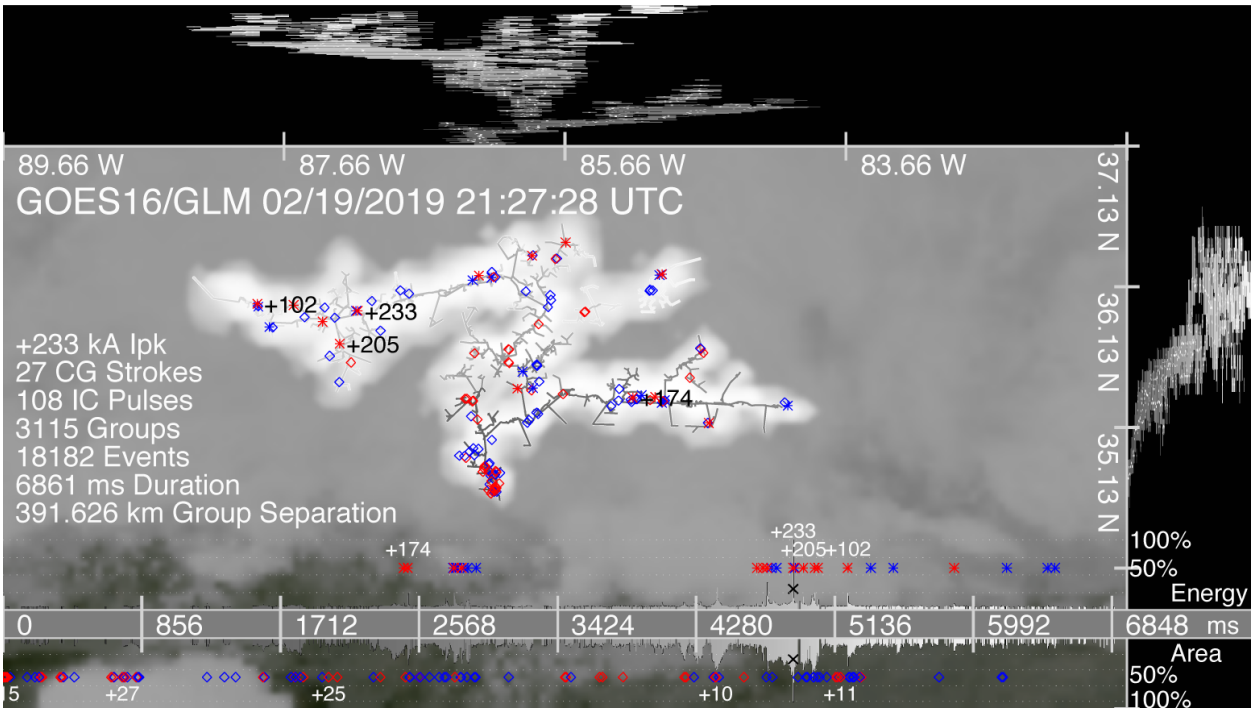

Figure 3. As in Figure 2, but for a stratiform 1000x superbolt case. Peak currents are only listed for CGs > 100 kA. ENGLN events occur along each branch in the lateral structure traced out by GLM groups.

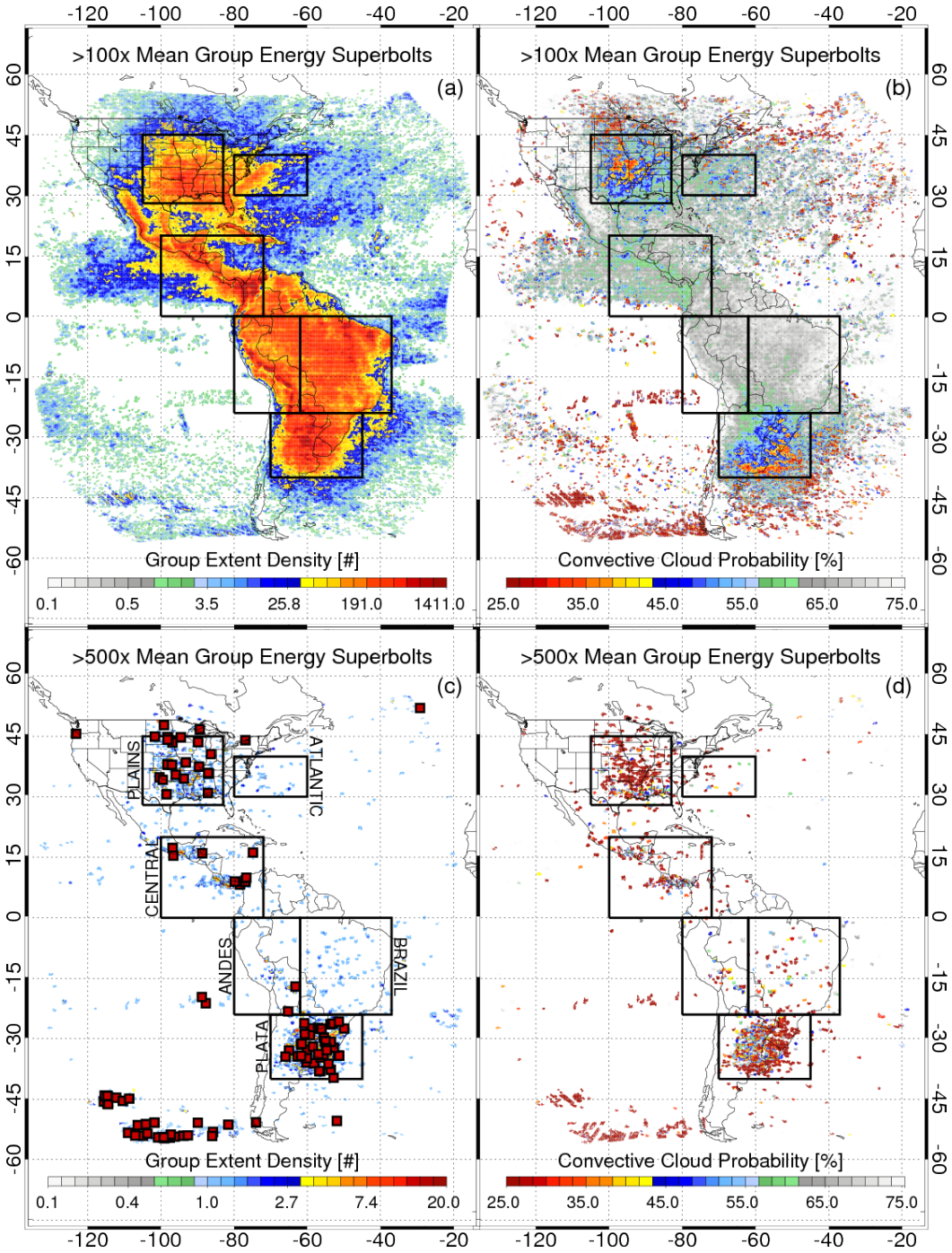

Figure 4. Global distributions of GLM superbolts at the 100x energy threshold level (a) and 500x threshold level (c), and average convective cloud probabilities for the superbolt cases at the 100x level (b) and 500xlevel (d). Regions of interest for subsequent analyses are outlined and named in (c). Red box symbols in (c) indicate the distribution of 1000x superbolts.

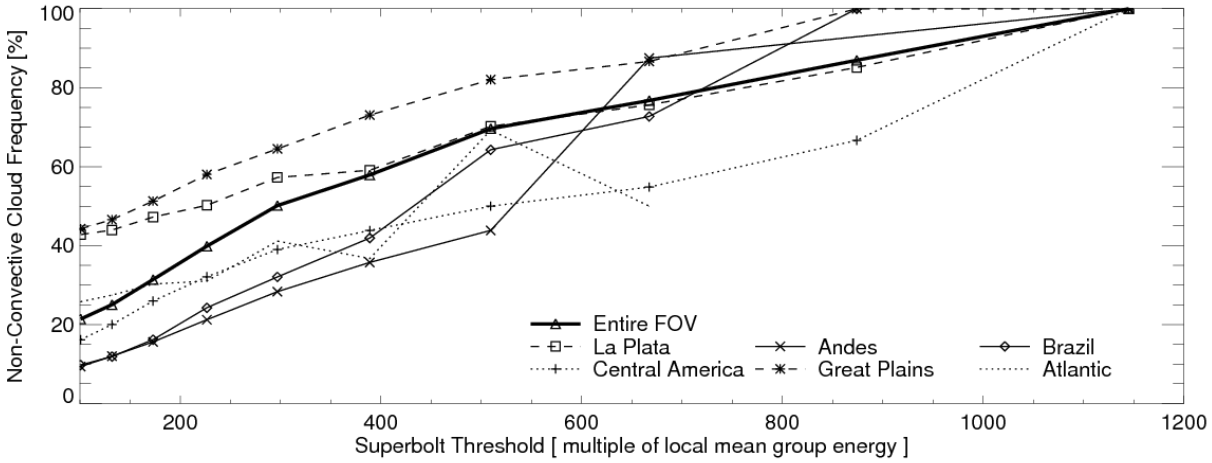

Figure 5b. Fractions of the superbolts in each region that occur in non-convective clouds at each superbolt threshold energy level.

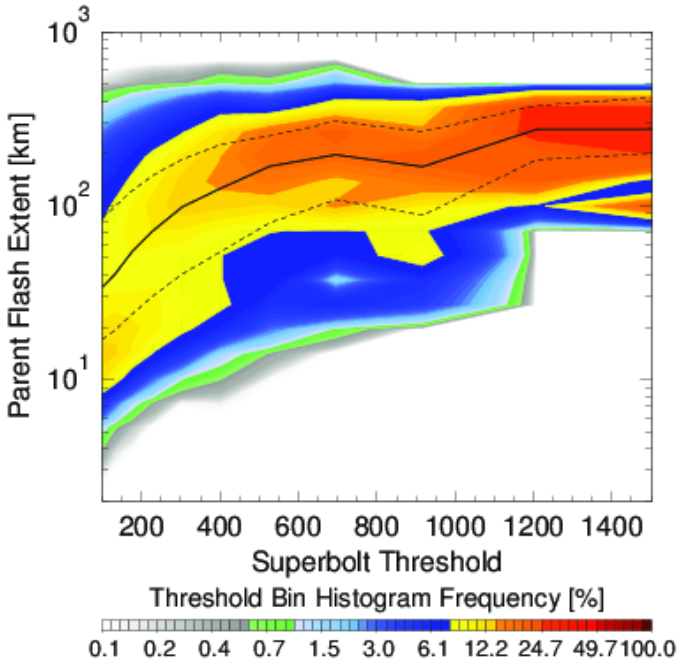

Figure 6. Histograms at each superbolt threshold energy level for the lateral extent of the parent GLM flash. Median (solid) and 25th and 75th percentiles (dashed) are shown as lines. At 100x, >75% of flashes that produce superbolts are not megaflashes (extent > 100 km). However, by 1000x, 75% of superbolt flashes are megaflashes.

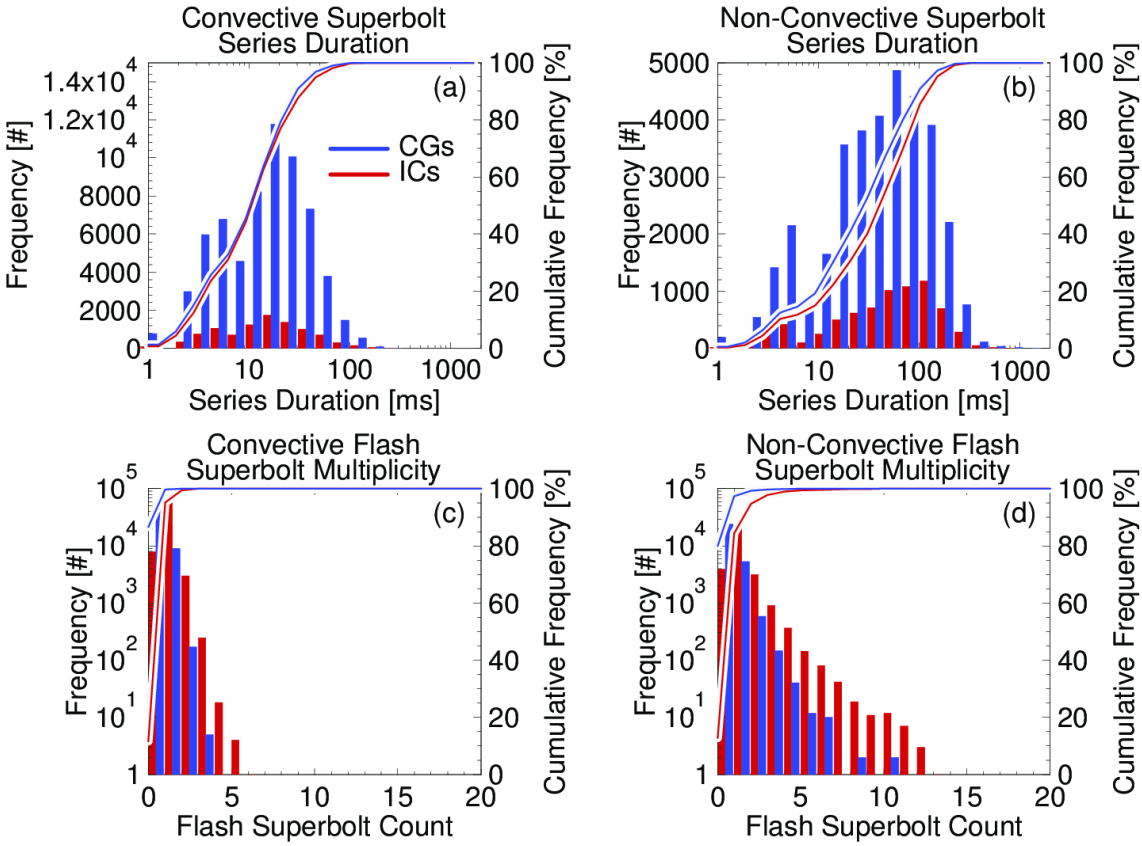

Figure 7. Distributions of the duration of the parent series for matched ENGLN superbolts (a-b) and the flash superbolt multiplicity (c-d). Histograms are shown as bar plots while CDFs are plotted with solid lines. Separate distributions are shown for superbolts in convective (a,c) and non-convective (b,d) clouds. Additionally, the sample is divided into CG cases (blue) an IC cases (red) in each panel.

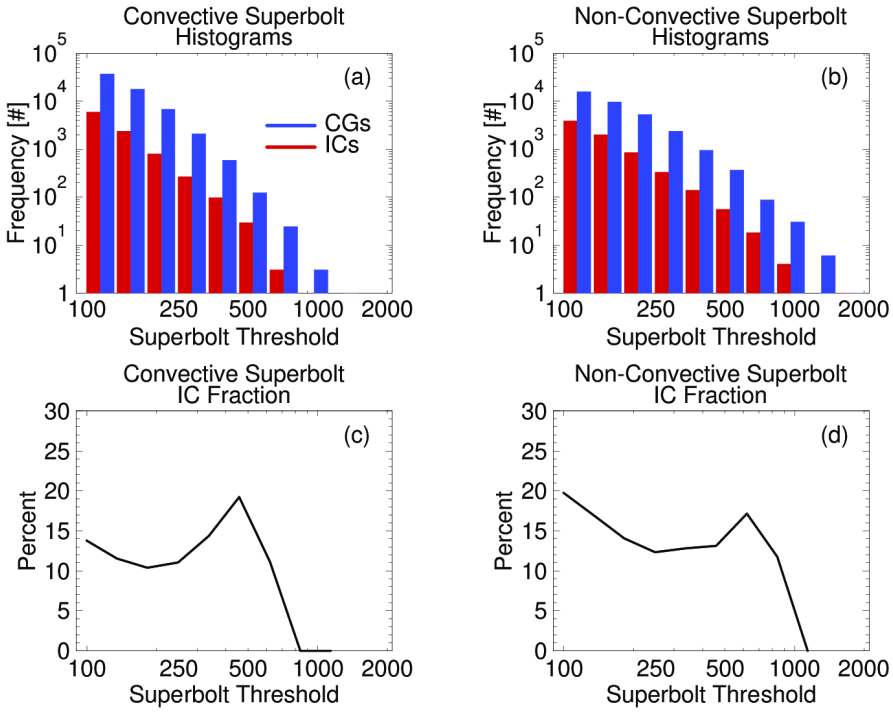

Figure 8. Histograms of CG and IC superbolt cases (a-b) and the IC fraction (c-d) at each energy level for convective (a,c) and non-convective (b,d) cloud types.

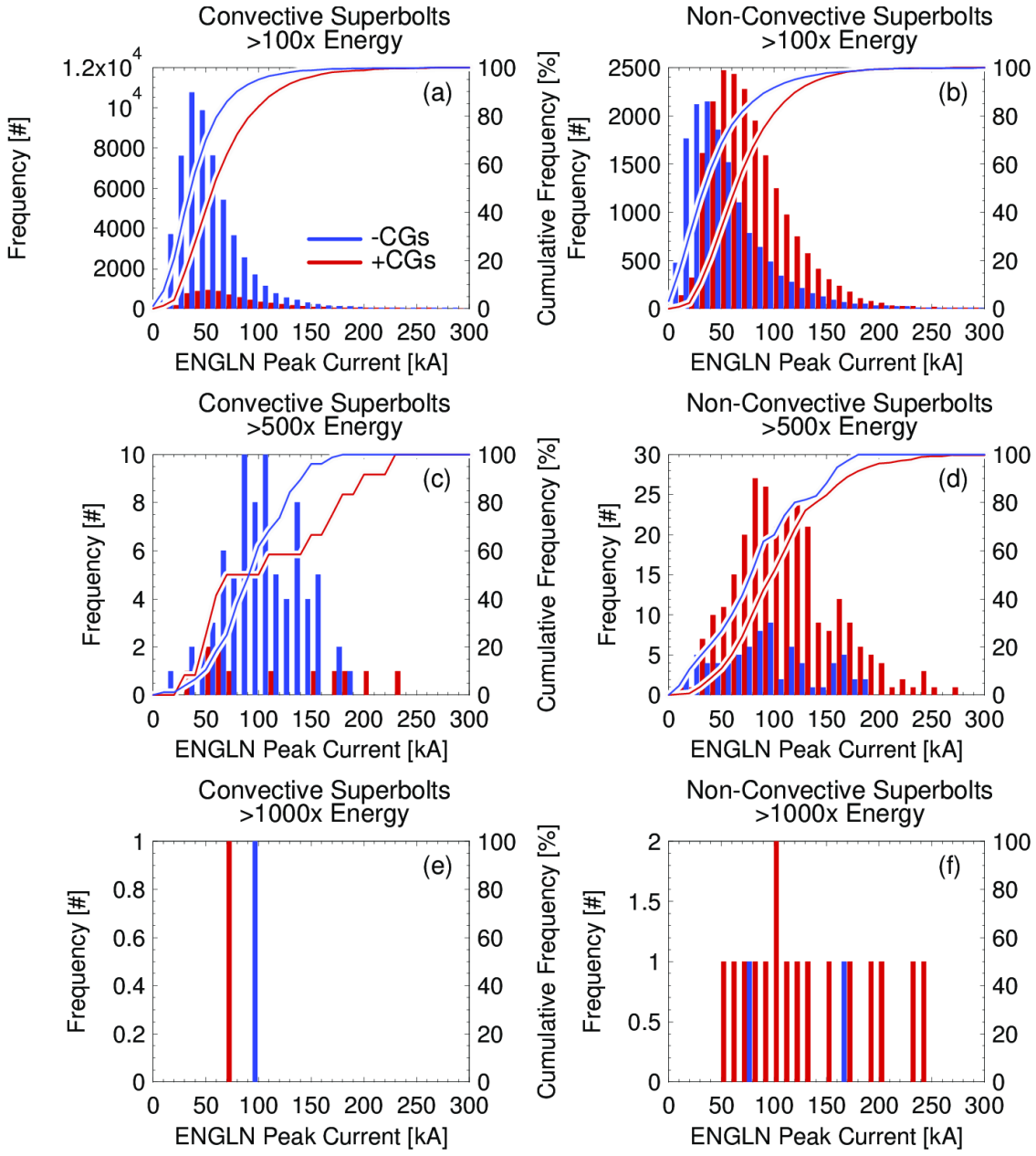

Figure 9. Distributions of CG superbolt peak current according to polarity (negative is blue while positive is red), GLM superbolt energy threshold (100x in a-c, 500x in c-d, and 1000x in e-f), and prevailing cloud type (convective in a,c,e, and non-convective in b,d,f).